Cellulose (2020) 27:6921–6933
https://doi.org/10.1007/s10570-020-03164-z

ORIGINAL RESEARCH

Analyzing the film formation mechanism of cellulose nanoparticles (CNPs) based on the fast freeze-drying morphology

Lanxing Du · Zhiming Yu · Jinwu Wang · Michael P. Wolcott · Yang Zhang · Chusheng Qi

Received: 11 December 2019 / Accepted: 10 April 2020 / Published online: 28 May 2020

Abstract The aim of this study was to discern the film formation mechanism of cellulose nanoparticle suspensions (CNP suspensions) by transforming the film formation process to be a water evaporation process, investigating the fast freeze-drying morphology of CNPs, the resulting natural formation structure, and the relationship of CNPs and water molecules. It was found that an increasing aspect ratio transforms CNPs from the oriented arrangement to a distributed network. Hydrogen bonds and van der Waals forces among CNPs led to a close and interactive film formation process, contributing to various microstructures in the resultant films. High aspect ratios in CNPs hindered the formation of interaction as well as increased absorbed water on CNPs. The interaction among CNPs, and the interaction between CNPs and water molecules were reflected in shear-thinning behavior of CNP suspensions. High aspect ratio CNPs had the capacity of absorbing more immobilized water, partially leading to a higher viscosity. The microstructures of CNP films were fund to be dense without significant layers or holes and varied from the fast freeze-drying morphology, due to the continuous volume reduction in water evaporation. Overall, it is expected that discerning the film formation mechanism of CNPs provide guidance for controlling the film structure and explaining the macroscopic property of the resultant materials.

L. Du
College of Forestry, Hebei Agriculture University, Baoding 071001, China

L. Du · Z. Yu (✉) · Y. Zhang · C. Qi
MOE Key Laboratory of Wooden Material Science and Application, Beijing Forestry University, Beijing 100083, China
e-mail: yuzhiming@bjfu.edu.cn

L. Du · M. P. Wolcott
Composite Materials and Engineering Center, Washington State University, Pullman, WA 99163, USA

J. Wang (✉)
Forest Products Laboratory, US Forest Service, Madison, WI 53726, USA
e-mail: jinwuwang@fs.fed.us

Graphic abstract

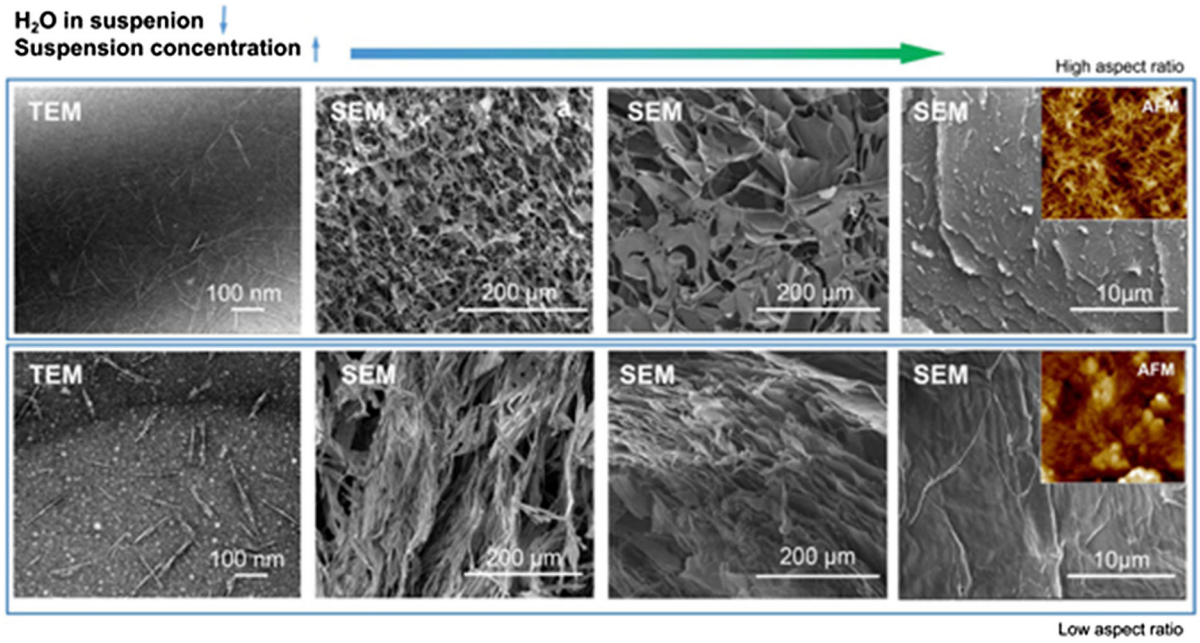

Keywords Cellulose nanoparticles · Aspect ratio · Film formation · Morphology · Viscosity

Introduction

Cellulose is the most abundant natural polymer resource brought from wood, cotton, wheat straw, bagasse, banana, rice husk, etc. The considerable amount of cellulose and its derivatives is able to be applied in a wide range of materials and products with an annual production of more than 7.5×10^{10} ton (Habibi 2014). The nano-scale cellulose is finding increased utilization (Ferrer et al. 2017). Their resulting films, hydrogels, aerogels, cooperated with polymers like PE, PP, PLA, PHBV or self-assembly moulding have fantastic mechanical, light, electrical, and barrier properties, thus leading to the research on nano-scale cellulose in depth (Mahfoudhi and Boufi 2017; Pircher et al. 2014; Eichhorn 2011; Sood et al. 2017; Ma et al. 2019; Chowdhury et al. 2018; Espino-Pérez et al. 2018; Lu et al. 2018).

Based on the physical structural features, the cellulose nanoparticles (CNPs) are divided into two types, cellulose nanocrystals (CNCs) and cellulose nanofibers (CNFs). The former possesses higher crystallinity and solid spindle-, or needle- like shapes, the latter has larger aspect ratio and irregular long fibers figures (Du et al. 2018; Fukuzumi et al. 2013). Various morphologies result in differences in the macroscopic property. CNCs present a higher transparency and CNFs are superior for interweaving flexible films and the gas barrier property (Rampazzo et al. 2017; Xia et al. 2018). These relationships indicate that CNP morphologies are the key factor affecting the resultant cellulose products. The resulting microstructures are based on their chemical groups and physical structures (Inamochi et al. 2017), depending on the film formation mechanism, especially for the CNP films. Therefore, understanding the CNP film forming mechanisms could help determine the relationship between structure and the resulting property and may provides new ideas in design and preparation of CNP products.

However, a problem appears in analyzing the film formation mechanism of CNPs. That is learning their film formation process. It is difficult to directly monitor the process by transmission electron microscope(TEM), scanning electron microscope (SEM), or polarized optial microscope (POM), due to the existence of water and the self-assembly property of the

CNPs. TEM or POM are able to observe the two-dimensional morphology at very low CNP concentrations (Errokh et al. 2018). In addition, SEM displays the three-dimensional morphology but requires a dry condition. The self-assembly property of CNPs hinder the dried CNP films reflecting the specific film formation process (Li et al. 2015). To solve this problem, we consider that the film formation process of the CNP suspension is equivalent to a water evaporation process, CNP concentrations continue to increase during the drying process. As a result, understanding the concentration of CNP suspensions during drying can delineate the film formation process. The evaporation and sublimation of water have the similar transport pathway, while existing the volume changes. Observing morphology evolution during the fast freeze-drying process can simulate the film formation process, and resolve the water problem in SEM observation. Certainly, the different water phase transition will develop the variety in physiochemical factors acting on film formation.

Therefore, the aim of this work is to discern the film formation process of CNP suspensions via the fast freeze-drying process. Here, we investigate the influence of CNP size on the resulting film microstructure, exploring the differences between fast freeze-drying morphology and natural dried CNP morphology in delineating the film formation process, and summarizing the film formation mechanism of the CNP suspensions. It is expected that determining the details of CNP microstructure provides guidance for controlling their structure and understanding the macroscopic property of the resultant materials.

Materials and methods

Raw materials

Cellulose nanocrystals (CNCs, gel, ~ 11.8% solids) and cellulose nanofibers (CNFs, slurry, 2.8% solids) were acquired from the University of Maine, USA. Microcrystalline cellulose (MCC) was purchased from Sigma-Aldrich Inc., USA. Three T-CNPs (TEMPO-oxidized cellulose nanoparticles, T-CNPs), including TEMPO-oxidized CNC (T-CNC), TEMPO-oxidized MCC (T-MCC), and TEMPO-oxidized CNF (T-CNF), were prepared by using our previous method (Du et al. 2018). In brief, TEMPO/NaClO/NaBr system were employed to oxidize types of celluose, the oxidation was stopped by adding alcohol and then was neutralized by diluted HCl solution titration. The resulting T-CNPs was washed and condensed by repeated centrifuging before testing. All samples were marked as CNPs.

Preparation of CNP films

All CNP dispersions were diluted to the concentrations of 2 wt%. The concentrated suspensions were cast into plastic petri dish (10 cm × 10 cm), followed by evaporation to form self-assembled films at room temperature. These suspensions were covered on the petri dish by plastic wrap with tiny holes to eliminate dust and facilitate airflow.

Zeta potential

A Malvern 3000 Zetasizer Nano ZS (Malvern Instruments Ltd., Worcestershire, UK) was used to determine the electrophoretic mobility of the starting materials and the CNP dispersions at a concentration of 0.005 wt%. The detecting angle was 173° and the wavelength was 633 nm.

SEM

The film surfaces and the fast freeze-drying morphology of various concentrations of CNP suspensions were characterized by SEM (FEI SEM Quanta 200F, USA) under high vacuum mode with an accelerating voltage of 5 kV. The dried samples were gently fixed on aluminium stubs with carbon adhesive disks.

TEM

CNC gel, CNF slurry, and the prepared T-CNP dispersions were diluted to the concentration of 0.01 wt%. The diluted dispersions were sonicated 10 min for homogeneous dispersing, and then the sonicated dispersions (5-μL) was deposited on a formvar- and carbon-coated copper grid and was stained by uranyl acetate (1 wt%) until the water completely evaporated. The sample morphology was imaged by JEOL 1200 EX transmission electron microscope (TEM, TEOL, Japan) with an accelerating voltage of 5 kV.

Aspect ratio

The aspect ratio (length to diameter, L/d) of samples were obtained by measuring the length and diameter of 100 individual particles from the TEM images, the average aspect ratio and the standard deviation were calculated and analyzed by ImageJ software and Excel.

AFM

The suspensions (0.5 wt%) were deposited on mica surface under ambient conditions until totally drying. After the self-assemble films were formed, the surfaces morphology of dried films were examined by atomic force microscope (Bruker Multimode 8, USA) using trangle-shaped cantilevers (spring constant, 0.06 Nm^{-1}). The film roughness was measured from AFM images by using NanoScope Analysis software.

Viscosity measurements

All CNP dispersions were diluted to the concentrations of 2 wt% and sonicated for 5 min to form a uniform suspension. Their viscosities were measured using a cone-plate MCR 302 rheometer (Anton Paar GmbH, Austria) at a shear rate ranging from 0.1 to 1000 s^{-1} at 25 °C. The cone diameter was 50 mm with the gap fixed at 0.01 mm and a cone angle of 1°.

Results and discussion

Morphology of CNPs in suspensions

TEMPO oxidation produced needle-like CNPs with very high aspect ratios (long to diameter, L/d) (Fig. 1 and Table 1). The oxidized CNPs produced a sufficient surface charge to homogeneously disperse themselves in diluted suspensions. The average aspect ratio value were as follows: T-CNFs > T-MCCs > T-CNCs > CNCs. CNCs with bundle-like shapes represented a collection of individual fibers with enlarged diameter, leading to a relative low aspect ratio. T-CNFs had a high zeta potential value of − 75 mV, resulting from the oxidation of reaction sites. The high aspect ratio may present more opportunity for oxidation of chemical groups.

Fast freeze-drying morphology of CNP suspensions

TEM images were acquired by using 0.01 wt% concentration of CNP suspensions for two dimensional observation. The diluted suspensions were not able to effectively allow fibers aggregate and entangle to form a continuous film. Compared to TEM images, the SEM image of T-CNFs show a three-dimensional network structure (Fig. 2a, b). At low concentrations, adjacent T-CNFs with large fiber angles formed a staggered structure. Hydrogen bonds and van der Waals forces led to T-CNFs with small fiber angles to interact, forming the fiber bundles or ribbon-like structure with a diameter range of 100–700 nm. Since the CNP size distribution determined the existence of tiny cellulose particles, these small cellulose were aligned to form ribbon-like film structures between the T-CNFs (Fig. 2c). The T-MCCs and T-CNCs displayed the bundle-like fiber structure with a diameter range of nano- to micro- meters (Fig. 2e, f, i). Meanwhile, the dried T-MCCs and T-CNCs were oriented. The CNCs (Fig. 2k) presented sheet and laminating morphology even at low concentrations. This behavior resulted from a comprehensive consideration of the aspect ratio, suspension concentration, hydrogen bonding, surface charge, etc. (Li et al. 2015; Han et al. 2013). A low aspect ratio and sufficient hydroxyl groups were prone to be oriented and aligned. Thus, once the suspensions exceeded the critical concentration, the CNCs firstly formed the thin film structure by surface hydrogen bonding and mutual repulsion.

At the high concentration, the laminated morphologies for T-MCCs, T-CNCs, and CNCs displayed a smooth surface in each layer, and the freeze-dried T-CNCs have more layers per unit thickness than T-MCCs, resulting from their small particle size (Fig. 2g, j, l). T-MCC layers were occasionally observed several irregularly distributed pores (Fig. 2g), these pores might attribute to channels for water transport gradually constructed during the sublimation process. As the T-MCCs and T-CNCs had relatively small aspect ratios, their CNPs were aligned as sheets with increasing length and width, finally being deposited as the well-organized structure and also being formed layer-by-layer through the repulsive force. However, the concentrated T-CNFs based on the network structure continued to be

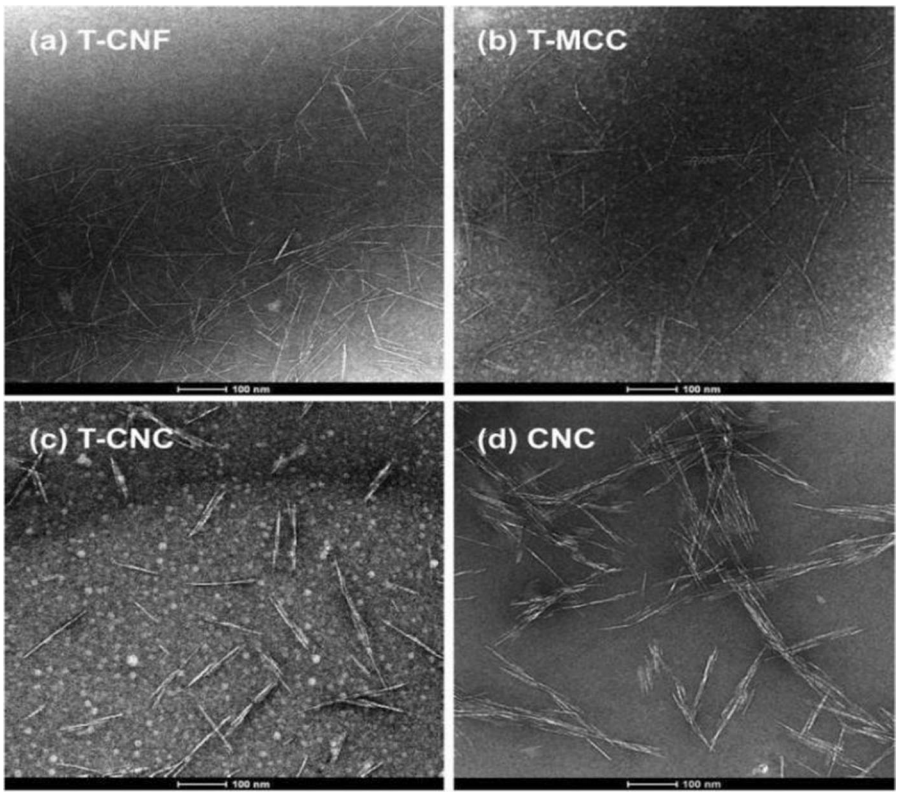

Fig. 1 The TEM images of CNPs (**a** T-CNF; **b** T-MCC; **c** T-CNC; **d** CNC)

Table 1 The average aspect ratios of CNPs

CNP samples	Average (L/d)	Zeta potential value (mV)
T-CNF	54.4(36.4)	−75
T-MCC	28.1(14.5)	−70
T-CNC	20.6(11.9)	−72
CNC	14.0(7.6)	−68

The value in bracket is the standard deviation

deposited as a porous foam with a partial of unclosed holes, and constructed layered arrangement by surface repulsive force (Fig. 2d). As a result, the concentrated CNP morphology displayed a significant variation in microstructure.

Evaluating the fast freeze-drying process

As precise imaging instruments are difficult to directly monitor the film formation process of a CNP suspension, the film formation process could be simulated as a water evaporation process with increasing concentration until complete evaporation. The water evaporation (liquid to vapor) and sublimation (solid to vapor) possessed similar transport pathway. Therefore, we expect to learn the water transport process and the film formation mechanism of CNPs by observing morphology development in fast freeze-drying of increasingly concentrated CNP suspensions. This process will help to simulate the similar film formation process and mechanism in the prediction of solvent loss process.

The fast freeze-drying process included two parts, freezing and drying. The CNP suspensions before freezing exhibited homogeneous and stable dispersions, owing to the negative charge via the carboxyl groups and sulfate groups on CNP surfaces. During the freezing process, the ice crystals gradually grew in the direction of the temperature gradient, that is, the ice crystals generated the layered microstructure parallel to the movement of freezing front (Han et al. 2013). The expanded volume required the CNPs to be squeezed and expelled into the space between ice

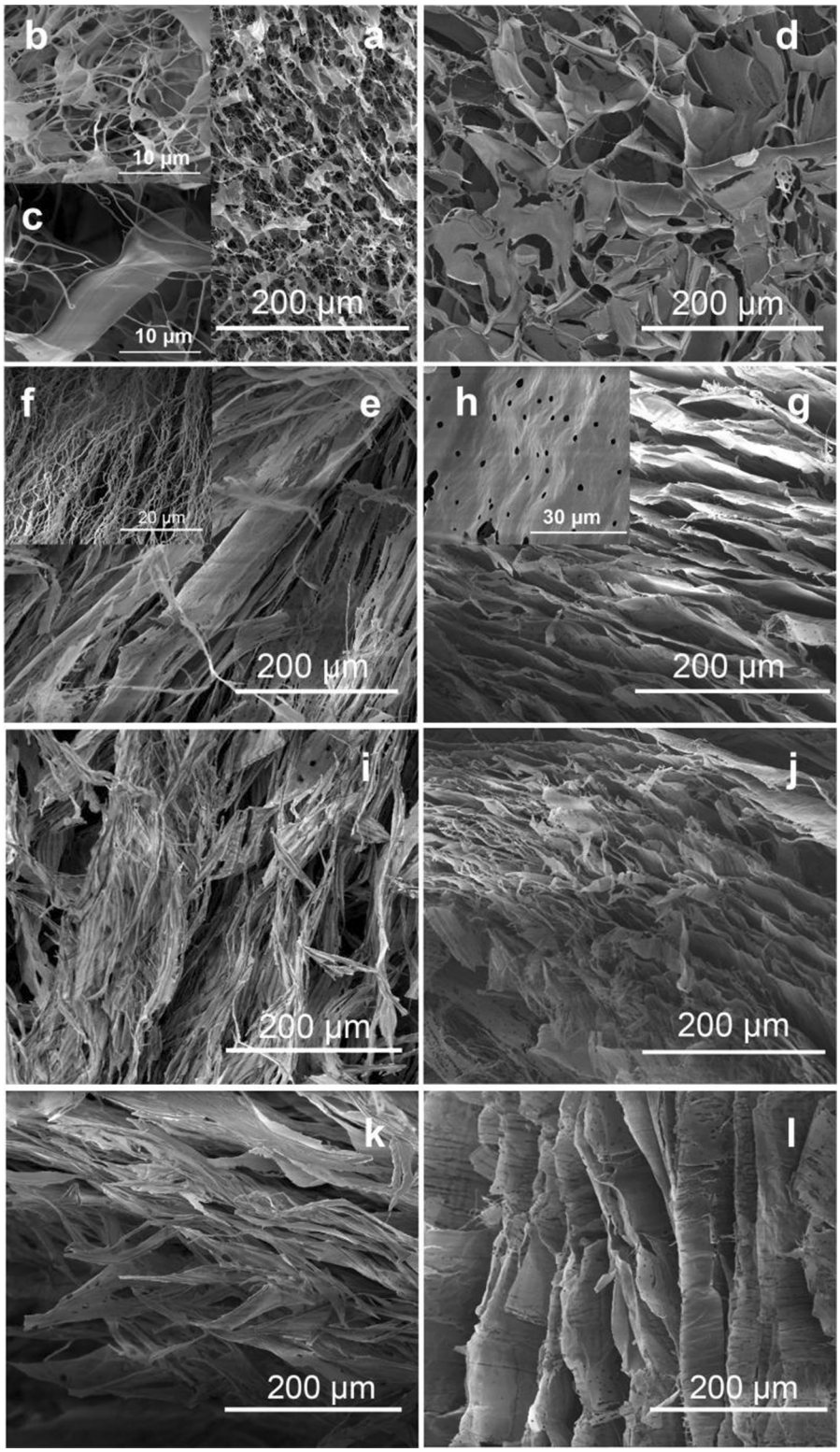
b
10 µm
a
c
10 µm
200 µm
d
200 µm
f
20 µm
e
200 µm
h
30 µm
g
200 µm
i
200 µm
j
200 µm
k
200 µm
l
200 µm

◀**Fig. 2** The SEM images of the CNPs after freezing drying, **a**, **b**, **c**, **d** T-CNF; **e**, **f**, **g**, **h** T-MCC; **i**, **j** T-CNC; **k**, **l** CNC (the concentration of a, b, c, e, f, k 0.3 ∼ 0.5 wt %; d, g, h, j, l 1.0 wt %)

fronts and ice sides, as shown in Fig. 3a. Once the original suspension exceeded the critical concentration for the ordered nematic phases, it led to the CNPs increasing in size and CNPs spontaneously forming the oriented structure along the ice crystals. When the freezing process was complete, the homogeneous CNP suspensions were transformed into an ice-template structure. Under the − 51 °C drying condition, ice was gradually sublimated, the CNPs retained the original frozen morphology and replicated the ice structure. The squeezed CNPs were realigned and self-assembled into microfibers by strong hydrogen bonds and van der Waals forces (Han et al. 2013; Lu and Hsieh, 2012). As a result, the fast-freeze drying morphologies of CNPs mainly depended on the freeze process.

For various aspect ratio, their suspensions exhibited different fast-freeze drying morpholgies. An analogous orientation appeared in T-MCC, T-CNC morphology. At the low concentration (0.3–0.5 wt%), the large spaces between T-MCC microfibers discouraged the formation of hydrogen bonds and interfacial attraction, resulting in the parallel arrangement of T-MCC microfibers and formation of a bundle-like morphology (Fig. 3b, d). Furthermore, the concentrated suspensions (1 wt%) decreased the fiber spacing and favored the orientation and self-assembly of microfibers into a compact sheet-like structure (Fig. 3c, e). In contrast, T-CNCs were prone to attract adjacent nanofibers and self-assembled a compact thin layer even at low concentration, due to the small particle size and abundant hydroxyl groups. This indicates that T-CNCs are prone to form a layer at low concentrations, and have the capacity of forming more layers per unit thickness (Fig. 2i). The CNCs displayed a similar process.

The T-CNFs had a network freeze-drying morphology, owing to their high aspect ratio and the high viscosity of the resulting suspension. A considerable amount of T-CNFs retained their original position in suspension and could hinder the ice crystal continued growth. Therefore, the ice crystals grew through the T-CNFs. With the ice crystal increasing growth, the squeezed T-CNFs were oriented into larger-sized cellulose microfibers and retained the original structure in suspension (Fig. 3f, h). The large gaps between ice crystals promoted the linkage of adjacent large microfibers and the formation of the ribbon-like layer at low concenration. The staggered and oriented T-CNFs coexisted at this condition. For the concentrated T-CNF suspension, the homogeneous T-CNFs were partially aligned by ice crystals along the temperature gradient during the freezing process, prohibiting the ice crystals from continuously growing, forming polyhedrons or spheres, and resulting in the staggered structure of T-CNF after freeze-drying (Fig. 3f, h). When the concentration further increased, the holey pathway generated by staggered structure were gradually filled and closed, the suspension was

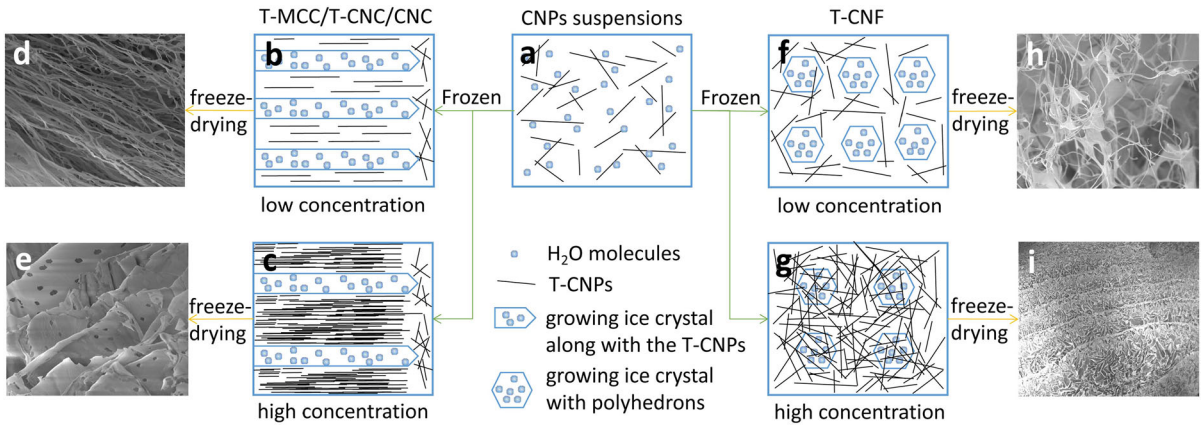

Fig. 3 The schematic of possible formation mechanism of the orientation of T-MCC, T-CNC, CNC, the network of T-CNF, and lamellar geometry during freeze-drying (d, e, h, i, were SEM images)

finally transformed to be a continuous porous foam (Fig. 3i).

Evaluating the film formation mechanism of CNP suspensions

Based on analyzing the fast-freeze drying process and the resulting CNP morphology, the natural film formation process of the CNP suspensions were deduced and evaluated. It was divided into two types: (1) CNPs with high aspect ratios and (2) CNPs with relatively low aspect ratios.

The suspension of high aspect ratio CNPs generally displayed high viscosity and shear-thinning behavior (T-CNFs). Water movement and evaporation almost had little influence on the original T-CNF position in suspension and the angles between individual T-CNF. This film formation morphology resulted from the physiochemical characteristics of the CNPs, including aspect ratio, surface charge, and flexibility. However, compared to the influence of high aspect ratio, hydrogen bonds between CNPs, absorbed water molecules and the chemical interaction between CNPs were weak (Li et al. 2015). Here, the aspect ratio was the key factor, affecting the film formation process and the resulting structures. During evaporation, the space between T-CNFs was gradually reduced, resulting in their suspension concentrations continuously increasing and an increased viscosity. Adjacent T-CNFs with a small angle and T-CNFs with a relative low aspect ratio were gradually assembled. The major of T-CNFs with a larger angle retained the original morphology, resulting in the original structure almost completely preserved. The sublimation had a volume increasing process before decreasing brought by the water to ice transition. Therefore, based on the staggered structure of the fast freeze-drying morphology, the T-CNF formed a dense film while without significant holes in three dimensions, owing to the gradually decreasing volume. Figure 4a shows the microstructure of a naturally evaporated T-CNF film, the T-CNFs are randomly arranged to be network structure with gaps between fibers, according with the evaluation of the T-CNF film formation.

Figure 4b–d depict films from CNPs with relative low aspect ratio, e.g. T-CNC, whose particles assembled into microfibers with parallel arrangement. The microfibers were naturally linked to form aligned sheets with the continuous reduction of the water. During the evaporation, the relatively low aspect ratio of CNPs allowed the surface charge and chemical interaction to play an important role in film formation, in contrast to from the T-CNFs. Hydrogen bonds caused the crystals to organize into parallel structrue and reduce the space between crystals. The remarkable layered structure of the freeze dried sample disappeared during natural evaporation. As a result, the CNPs with relative low aspect ratio finally formed an aligned dense film. Figure 4b–d, shows the microstructure of natural evaporated T-MCC, T-CNC, CNC. The T-CNC and CNC were well-organized. T-MCC film displayed a microstructure between T-CNF and T-CNC, they coexisted the organized arrangement and the random structure. It was due to the increasing aspect ratio. CNC, T-CNC, T-MCC presented an increasing average aspect ratio value of 14.0, 20.6, 28.1, respectively, corresponding with the exhibited fiber angles between CNPs and the transition from an orientated to a network structure. It indicated the higher aspect ratio, the more random the network structure.

The moisture content in suspension determined the water transport pathway. According to the BET theory and Dent theory, it was supposed that water molecule exist two states in CNP suspension, the absorbed water molecule and the free water molecule (Branaver et al. 1938; Dent 1980; Skaar 1988). The absorbed water was locked on the surfaces of CNPs layer-by-layer through the physiochemical interaction. The closest absorbed water molecule (primary absorbed water molecule) had the strongest interaction, like hydrogen bonding. It was difficult to remove in evaporation. The outer layer with secondary absorbed water molecules was prone to transport (Fig. 5a, b). Therefore, high aspect ratio CNPs (T-CNFs) resulted in the increase of absorbed water (Fig. 5c, d). The remaining free water molecule moved along with the aqueous phase until totally disappeared. The resultant moisture content gradient made CNPs with small fiber angles be gradually close, while high aspect ratio caused inevitable steric hindrance with each other, preventing the gradual organization, except introducing sufficient external force to change the direction (Fig. 5e). On the other hand, it could be considered that the function of the interconnection of CNPs and the ability of CNPs to rotate in the thickening fluid had the strong influence on the resultant structures. The smaller or lower aspect ratio CNPs had a more easily rational inertia than the

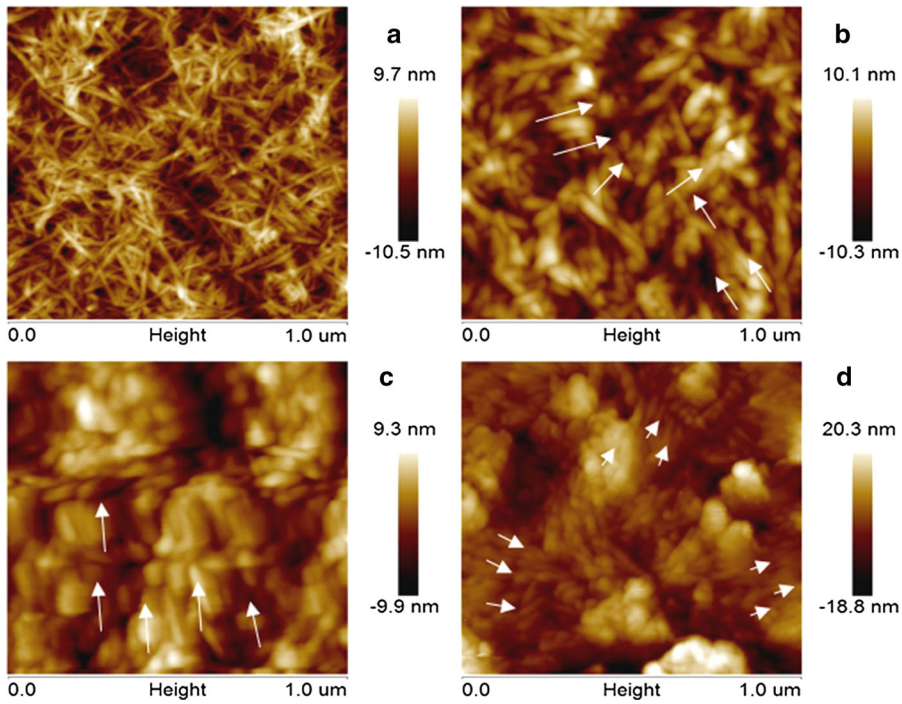

Fig. 4 The surface morphology of the CNPs suspensions after natural evaporation; AFM images: **a** T-CNF; **b** T-MCC; **c** T-CNC; **d** CNC

longer or higher aspect ratio CNPs. Meanwhile, the immobilized absorbed water molecules covered the CNPs, possibly hindering the further affraction and the formation of hydrogen bonds. However, insufficient aspect ratio (T-CNC, CNC) does not interfere with organization, moisture content gradient and water vapor pressure provide a driving force to rotate CNPs into a parallel orientation. Therefore, the resultant microstructures were determined by cooperation of aspect ratio and the interaction. The water transport pathway was summarized as water movement in free water region and the water migration on CNP surfaces. It is known that all sample has the aspect ratio distribution with a large particle size range, and their suspension has water transport pathways everywhere, easily appearing the differences in moisture movement over a large volume. The migration of free and absorbed water molecule usually coexisted in the whole evaporation process.

During the film formation process, the gradually increased concentration of CNP suspensions generated increased steady-state viscosity (Du et al. 2018). This viscosity reflected the internal friction force when CNPs moving, the relationship between CNPs, and the relationship between CNPs and water (Fig. 6). In steady-state flow, the suspensions were considered to be a combination of many fluid layers moving parallel to each other (Fig. 7) (Cheng and Schachman 1955). Various speeds of fluid layers generated the shear rate, and the friction force between the layers developed the shear force. The rheological curve reflected the variation relationship of shear rate and shear force. Due to the small molecular weight, water molecule was subjected to a shear force equally to shear rate, showing a Newtonian fluid property. All free water molecule moved along shear direction over the whole shear rate range. The absorbed water on CNPs required extra driving force to move. In other words, CNPs with the absorbed water needed to overcome the enhanced friction force to flow in layers. It resulted in the increase of viscosity. Due to the thixotropic property of CNPs, with the increase of shear rate, the absorbed water molecule was converted into free water molecule, and the CNPs were gradually moved and aligned as much as possible in the direction of shear force, leading to the decrease of viscosity. Hence, the CNP suspensions showed one of pseudoplastic fluid property, i.e. the shear-thinning behavior. Obviously, the film formation process was a slowly water evaporation process, differing from the steady-state viscosity test by generating the shear force rapidly, the CNP suspensions were always in a state of

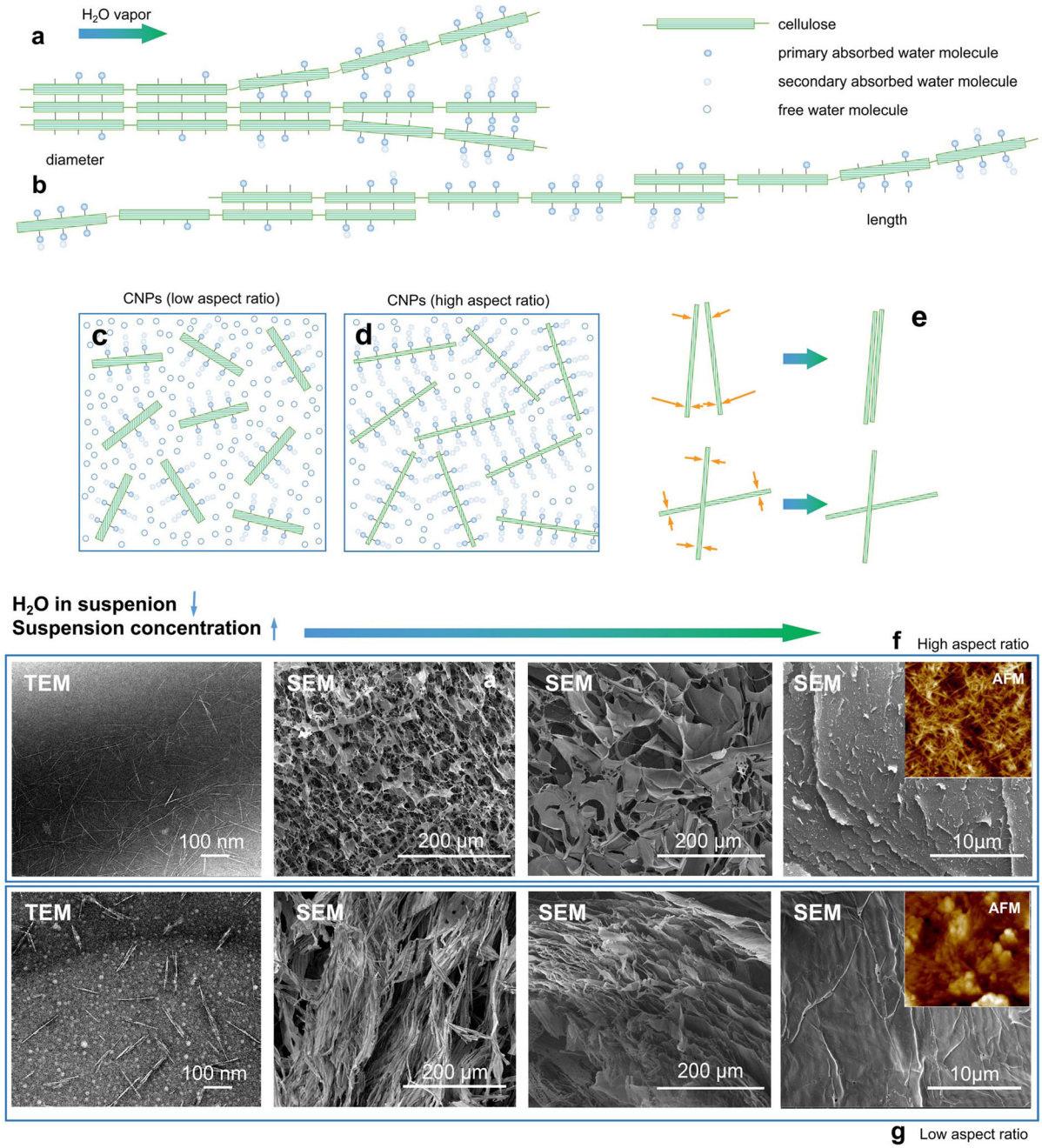

Fig. 5 The schematic illustration of film formation of the CNP suspensions (CNP orientation with the water movement, **a** size enlarged in width, **b** size enlarged in length; the possible statement of CNPs and the water molecules in suspension below the critical concentration, **c** low aspect ratio; **d** high aspect ratio; **e** the changes of CNP directions during evaporation; the film formation proces, **f** high aspect ratio, **g** low aspect ratio)

relative high viscosity under low shear rate. At this time, high aspect ratio exposed more free groups at the same concentration. It absorbed more water molecules as absorbed water, leading to difficultly overcoming their original structure, even rotation, when these immobilized water molecules and CNPs were as a integrated unit to move. As a result, T-CNF suspension had a high value of rehological curve. The high

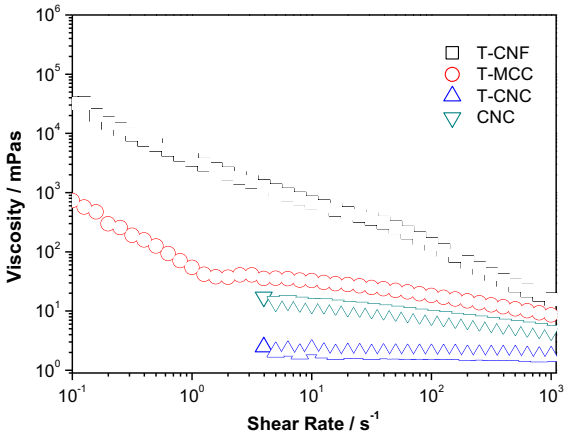

Fig. 6 The steady-state viscosity of concentrated CNP suspensions at 25 °C. The steady-state viscosities at low concentrations and the low shear rate could not be accurately detected due to the precision of the instrument

friction was generated to hinder the movement and rotation of CNPs. The resultant T-CNF almost kept the original network structure. On the contrary, CNC with relative low aspect ratio were easy to rotate in water layers and form hydrogen bond with close distance, the resulting films were parallel arrangement. T-CNC and T-MCC was somewhere between these two cases.

Besides the viscosity reflected the physical entanglement and chemical interaction between CNPs. CNPs gradually oriented along the shear direction at the low shear force, exhibiting a decrease of viscosity. Due to the big resistance among CNPs, specially the CNPs with high aspect ratio, they flowed slower than water with the increasing shear rate, the moving CNPs twisted and entangled with the static or slowly moving CNPs with the increase of shear rate, stopping the continuous reduction of viscosity. However, the increasing shear force was able to break the entangled network to be individuals, the CNPs gradually oriented along the shear direction, continuously dropping the viscosity (Fig. 7). The entanglement process made the CNP suspensions exhibited a three-region shear-thinning behavior. As a result, individual CNP would mutual restrict, movement and rotation in water become more difficult. Instead, the low aspect ratio CNPs, like T-CNC, was prone to orientation, the suspension had a continuously decreasing viscosity with the shear rate increasing.

The negative charge had the contribution in film formation. However, all CNPs were in a narrow arrange from − 68 to − 75 mV, the differences between each type of CNPs were limited. The viscosity indirectly demonstrated that the aspect ratio played a key role in entanglement, hydrogen bonding forming, and fiber rotation, thus, determining the film formation. As a result, the negative charge would not be additionally discussed except the aspect ratio in a similar range.

Conclusion

In this work, the film formation mechanism of CNP suspensions were explored based on evaluating the fast freeze-drying process, the natural film morphology, and the relationship of CNPs and water molecules. The different microstructures of CNPs depended on the cooperation of aspect ratio of CNPs and the interaction between CNPs. With the gradual water evaporation, high aspect ratio made CNPs from keeping their original positions as the staggered structure, depositing as a porous structure, to being a dense film with network structure. CNPs with low aspect ratio were oriented to be laminating morphology, gradually forming a well-organized dense film. Meanwhile, the increasing aspect ratio could transform the resulting films from the oriented arrangement to the network structure. The high aspect ratio hindered the formation of interaction as well as the absorbed water on CNPs. During film formation CNPs

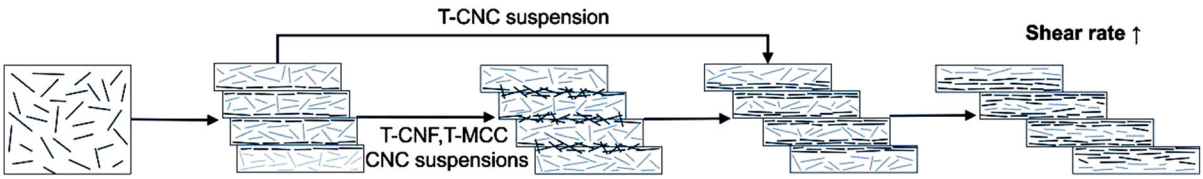

Fig. 7 The schematic of rheological behavior of CNP suspensions

were gradually close and interactive by hydrogen bonds and van der Waals forces. The rheological property of CNP suspensions reflected the interaction between CNPs, and the interaction between CNPs and water molecules by exhibiting linear or curve shear-thinning behavior. Since the sublimation include a process of volume expansion, the fast freeze-drying morphology exhibited significant layers and holes, the natural film morphology formed a dense microstructure, due to the continuously reduced water volume in phase transition. Therefore, a controlled structure can be designed by adjusting the aspect ratio, providing the guidance for preparing novel composites and helping understanding their macroscopic property.

Acknowledgments This study was financially supported by the Fundamental Research Funds of the Central Universities (The Open Fund of MOE Key Laboratory of Wooden Material Science and Application, Beijing Forestry University, No. BJFUKF201905), Natural Science Fund of Hebei Province (No. C2019204340), Science Research Fund of Hebei Agriculture University (No. YJ201820), and Forestry Science Group Fund of Hebei Agricultural University. The authors were also grateful to financial support from the Agriculture and Food Research Initiative (AFRI) Competitive grant (No. 2011-68005-30416), USDA National Institute of Food and Agriculture (NIFA) through the Northwest Advanced Renewables Alliance (NARA).

References

Branaver S, Emmeff P, Teller E (1938) Adsorption of gases in multimolecular layers. J Am Chem Soc 60:309–319. https://doi.org/10.1021/ja01269a023

Cheng Y, Schachman K (1955) Studies on the validity of the Einstein viscosity law and Stokes' law of sedimentation. J Polym Sci 16(81):19–30. https://doi.org/10.1002/pol.1955.120168102

Chowdhury R, Clarkson C, Youngblood J (2018) Continuous roll-to-roll fabrication of transparent cellulose nanocrystal (CNC) coatings with controlled anisotropy. Cellulose 25(3):1769–1781. https://doi.org/10.1007/s10570-018-1688-4

Dent R (1980) A sorption theory for gas mixtures. Polym Eng Sci 20(4):286–289. https://doi.org/10.1002/pen.760200411

Du L, Zhong T, Wolcott M, Zhang Y, Qi C, Zhao B, Wang J, Yu Z (2018) Dispersing and stabilizing cellulose nanoparticles in acrylic resin dispersions with unreduced transparency and changed rheological property. Cellulose 25(4):2435–2450. https://doi.org/10.1007/s10570-018-1739-x

Eichhorn S (2011) Cellulose nanowhiskers: promising materials for advanced applications. Soft Matter 7(2):303–315. https://doi.org/10.1039/c0sm00142b

Errokh A, Magnin A, Putaux J, Boufi S (2018) Morphology of the nanocellulose produced by periodate oxidation and reductive treatment of cellulose fibers. Cellulose 25(7):3899–3911. https://doi.org/10.1007/s10570-018-1871-7

Espino-Pérez E, Bras J, Almeida G, Plessis C, Belgacem N, Perré P, Domenek S (2018) Designed cellulose nanocrystal surface properties for improving barrier properties in polylactide nanocomposites. Carbohydr Polym 183:267–277. https://doi.org/10.1016/j.carbpol.2017.12.005

Ferrer A, Pal L, Hubbe M (2017) Nanocellulose in packaging: advances in barrier layer technologies. Industrial Crops Products 95:574–582. https://doi.org/10.1016/j.indcrop.2016.11.012

Fukuzumi H, Saito T, Isogai A (2013) Influence of TEMPO-oxidized cellulose nanofibril length on film properties. Carbohydr Polym 93(1):172–177. https://doi.org/10.1016/j.carbpol.2012.04.069

Habibi Y (2014) Key advances in the chemical modification of nanocelluloses. Chem Soc Rev 43(5):1519–1542. https://doi.org/10.1039/c3cs60204d

Han J, Zhou C, Wu Y, Liu F, Wu Q (2013) Self-assembling behavior of cellulose nanoparticles during freeze-drying: effect of suspension concentration, particle size, crystal structure, and surface charge. Biomacromol 14(5):1529–1540. https://doi.org/10.1021/bm4001734

Inamochi T, Funahashi R, Nakamura Y, Saito T, Isogai A (2017) Effect of coexisting salt on TEMPO-mediated oxidation of wood cellulose for preparation of nanocellulose. Cellulose 24(9):4097–4101. https://doi.org/10.1007/s10570-017-1402-y

Li M, Wu Q, Song K, Lee S, Qing Y, Wu Y (2015) Cellulose nanoparticles: structure-morphology-rheology relationships. ACS Sustainable Chem Eng 3(5):821–832. https://doi.org/10.1021/acssuschemeng.5b00144

Lu P, Hsieh Y (2012) Preparation and characterization of cellulose nanocrystals from rice straw. Carbohydr Polym 87:564–573. https://doi.org/10.1016/j.carbpol.2011.08.022

Lu P, Guo M, Xu Z, Wu M (2018) Application of nanofibrillated cellulose on BOPP/LDPE film as oxygen barrier and antimicrobial coating based on cold plasma treatment. Coatings 8(6):207. https://doi.org/10.3390/coatings8060207

Ma X, Deng Q, Wang L, Zheng X, Wang S, Wang Q, Chen L, Huang L, Ouyang X, Cao S (2019) Cellulose transparent conductive film and its feasible use in perovskite solar cells. RSC Adv 9(17):9348–9353. https://doi.org/10.1039/c9ra01301f

Mahfoudhi N, Boufi S (2017) Nanocellulose as a novel nanostructured adsorbent for environmental remediation: a review. Cellulose 24(3):1171–1197. https://doi.org/10.1007/s10570-017-1194-0

Pircher N, Veigel S, Aigner N, Nedelec M, Rosenau T, Liebner F (2014) Reinforcement of bacterial cellulose aerogels with biocompatible polymers. Carbohydr Polym 111:505–513. https://doi.org/10.1016/j.carbpol.2014.04.029

Rampazzo R, Alkan D, Gazzotti S, Ortenzi A, Piva G, Piergiovanni L (2017) Cellulose nanocrystals from

lignocellulosic raw materials, for oxygen barrier coatings on food packaging films. Packag Technol Sci 30(10):645–661. https://doi.org/10.1002/pts.2308

Skaar C (1988) Theories of water sorption by wood. springer series in wood science (Chapter 3), 86–121. https://doi.org/10.1007/978-3-642-73683-4_3

Sood S, Gupta K, Agarwal S, Dev K, Pathania D (2017) Controlled release of antibiotic amoxicillin drug using carboxymethyl cellulose-cl-poly(lactic acid-co-itaconic acid) hydrogel. Int J Biol Macromol 101:612–620. https://doi.org/10.1016/j.ijbiomac.2017.03.103

Xia J, Zhang Z, Liu W, Li F, Cao Y, Zhang W, Deng Y (2018) Highly transparent 100% cellulose nanofibril films with extremely high oxygen barriers in high relative humidity. Cellulose 25(7):4057–4066. https://doi.org/10.1007/s10570-018-1843-y